

---

# Study of Geometries and Electronic Properties of $\text{AgSi}_n$ Clusters Using DFT/TB

---

D. H. ZIELLA,<sup>1</sup> M. C. CAPUTO,<sup>1</sup> AND P. F. PROVASI<sup>2</sup>

<sup>1</sup>Department of Physics, Universidad de Buenos Aires and IFIBA, Ciudad Universitaria, Capital, Argentina

<sup>2</sup>Department of Physics, University of Northeast, Av. Libertad 5500, Corrientes, Argentina

Received 24 February 2010; accepted 19 April 2010

Published online 8 September 2010 in Wiley Online Library (wileyonlinelibrary.com).

DOI 10.1002/qua.22815

---

**ABSTRACT:** We present a theoretical study of the structures of silver silicon clusters,  $\text{AgSi}_n$ ,  $n = 1\text{--}15$ , using density functional tight binding methods. We discuss in detail the search for silicon clusters stabilized by silver dopage, their dissociation paths, and electronic properties. We also investigate the properties of silver encapsulated structures and compare them with those obtained when replacing the silver atom by different metals. Our results are checked against experimental measurements when available. © 2010 Wiley Periodicals, Inc. *Int J Quantum Chem* 111: 1680–1693, 2011

**Key words:** DFTB; doped-silicon clusters; polarizabilities; random search

---

## 1. Introduction

**S**ilicon is currently one of the most important materials for electronic devices. The study of the nanostructures it forms is motivated by their technological applications in microelectronics [1] and optics [2], for instance. Lately, there has been a significant amount of research concerning the synthesis of nanodevices in which small atomic clusters

constitute the elementary building blocks. Si clusters have been extensively studied using both theoretical and experimental techniques [3–5], and the interest in understanding their properties with miniaturization grows day by day.

A recent progress in nanostructures of silicon is the possibility to produce novel forms, such as silicon fullerenes and nanotubes using stabilization via metal encapsulation, to overcome the reluctance of silicon to form  $\text{sp}^2$  structures similar to those of carbon [6]. This development has revived the interest to understand the interactions of metal atoms with Si clusters and to search for cage-like Si clusters stabilized by metal atom incorporation. Hiura et al. have found experimental evidence of the formation of stable metal-encapsulating silicon cage cluster ions  $\text{MSi}_n$  [7]. This has been the starting point for

Correspondence to: M. C. Caputo; e-mail: caputo@df.uba.ar.

Contract grant sponsor: Universidad de Buenos Aires.

Contract grant number: UBACYT X-035.

Contract grant sponsor: FONCYT.

Contract grant numbers: PICTO-UNNE-227, PICTO-UNNE-204, BID-1728/OC-AR.

several computational investigations performed for metal-doped silicon clusters [8, 9]. Very recently, Kumar and Kawazoe [10–12] reported several types of metal-encapsulating caged structures with high stability for a series of MSi<sub>n</sub> clusters for  $n = 14$ – $17$  and M an element of the IVB–VIB or VIIB groups.

From these studies, it has become clear that the nature of the metal atoms and their interactions with Si plays an important role modifying the bonding and thereby the structure of the host cluster. In particular, coinage metal silicides have received much experimental attention due to their common use in electronic devices. For example, several studies have focused on the trends observed for silicide formation in Cu, Ag, and Au films deposited on silicon substrates [13–15].

Notwithstanding the general interest in metal-doped silicon clusters, the number of theoretical studies devoted to group IB metals (Cu, Ag, and Au) is surprisingly limited compared with similar systems involving other metal-doped silicon clusters [7, 9].

In the case of Ag, the first gas phase measurements of the dissociation energy for diatomic silver silicide were carried out by Riekert et al. [16], and the first evidence for the existence of polyatomic silver silicides was obtained by Scherer et al. [14]. They used cavity ringdown laser absorption spectroscopy (CRLAS) and time-of-flight mass spectroscopy (TOFMS) for the study of jet-cooled coinage metal silicides. Their results include the first gas phase spectra for any silver silicide.

The first experimental observation of photodissociation of silver-silicon clusters was carried out in 2006 by Jaeger et al. [12]. They reported that the most abundantly formed silver-silicon products turned out to be AgSi<sub>7</sub> and AgSi<sub>10</sub>. These two cluster sizes were prominent and no other mixed cluster was produced with high enough concentration for its photodissociation to be properly studied. They measured that the process occurs basically by the loss of metal atoms. This indicates that the metal is not located within the interior of silicon cages, and that the silicon-metal bonding is weaker on average than the silicon-silicon bonding. In fact, the most abundant fragment ions produced were Si<sub>7</sub><sup>+</sup> and Si<sub>10</sub><sup>+</sup>, for AgSi<sub>7</sub> and AgSi<sub>10</sub> respectively, indicating that the ionization potential (IP) of Si<sub>7</sub> and Si<sub>10</sub> clusters are lower than that of Ag.

A recent comparative study by Gueorguiev et al. [17, 18] on metal-doped silicon clusters found that AgSi<sub>10</sub> is endohedral, in contrast with the experimental results above. Lately, Zhang et al. [19] carried out

partial theoretical studies on AgSi<sub>n</sub> clusters ( $n = 1$ – $13$ ). Their results suggest that AgSi<sub>n</sub> clusters with  $n = 7$  and  $10$  are relatively stable isomers and that the Ag atom prefers to cap the Si clusters rather than be embedded inside it.

The goal of our article is to provide a systematic theoretical study of the equilibrium geometries, binding energies, and electronic properties of the silver silicides (AgSi<sub>n</sub> with  $n = 1$ – $14$ ). In addition we compare the most stable cages found, AgSi<sub>10</sub>, AgSi<sub>11</sub>, and AgSi<sub>12</sub>, to similar cages with different dopant metals like Al, Fe, Co, Ni, Cu, and Au.

In Section 2, we describe our computational methods. In Section 3, we present our calculations and analysis of different properties of AgSi<sub>n</sub> clusters,  $n = 1$ – $15$ : binding energy, hardness, electronic stability, and polarizability. In Section 4, we compare AgSi<sub>n</sub> ( $n = 10$ – $12$ ) cages to those with other metals as dopants. Finally, we summarize our conclusions and future prospects in Section 5.

---

## 2. Methodology

In the field of molecular physics the use of predictor/corrector schemes is very common. In these, local minima are looked for in a raw but efficient approach from the computational point of view, and then the search is refined with a more precise method.

To determine the best structures of AgSi<sub>n</sub>, we first apply the Random Search Algorithm (RSA), section 2.1, which implements the density functional-based tight binding (DFTB) [20] formalism, section 2.2. We then use the DFT method to refine the most promising RSA structures via a local optimization.

### 2.1. THE RANDOM SEARCH ALGORITHM

The random search algorithm (RSA) is the simplest method for finding minima on a potential energy surface. It involves performing a large number of searches from random starting points. For an  $N$ -atom cluster, we generate each structure by picking  $N$  sets of coordinates, according to the following prescription. Nuclei are chosen at random without reposition from the set of all species, counted with multiplicity. The first one is placed at the origin. The second nucleus is put in the neighborhood of the first one, satisfying maximum and minimum values for the distance between atomic species. Then, until the cluster is complete, each additional nucleus is

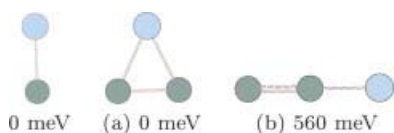


**FIGURE 1.** The lowest energy isomers of neutral  $\text{AgSi}_1$  and  $\text{AgSi}_2$ . The numbers under the structures are the relative energies with respect to the lowest energy isomer of the same size. The Si and Ag atoms are shown in dark blue (dark gray) and light blue (light gray) respectively. [Color figure can be viewed in the online issue, which is available at [wileyonlinelibrary.com](http://wileyonlinelibrary.com).]

positioned in the neighborhood of an already placed nucleus chosen at random from the building cluster taking care that

- no two atoms can be closer than  $r_{\min}$  ( $r_{\text{Si-Si}} = 2.3 \text{ \AA}$ ,  $r_{\text{Ag-Si}} = 2.4 \text{ \AA}$ ). This condition precludes starting geometries, which are too compressed, and hence very high in energy.
- the largest distance between an atom and its neighbors cannot be greater than a certain  $r_{\max}$  ( $r_{\text{Si-Si}} = 2.4 \text{ \AA}$ ,  $r_{\text{Ag-Si}} = 2.5 \text{ \AA}$ ). This prevents initial geometries in which one or more atoms are not connected to the remainder of the cluster.

The requisites invoked for the generator of structures were, in order, connectivity, nonsuperposition, simplicity, efficiency of implementation, and unbiasedness (in the sense that we do not tend to favor some topologies over others, such as for instance, compact over stretched or prolate geometries).

We applied the previous steps for  $\text{AgSi}_n$  clusters with  $n = 1-14$ . In the case of the  $\text{AgSi}_{15}$ , because of the unwieldy computational cost of a full configuration space study, we restricted ourselves to structures where the Ag atom is encapsulated within a Si cage. We implement this restriction within the random search algorithm by placing the silver atom at the origin of the coordinate system and adding Si atoms as

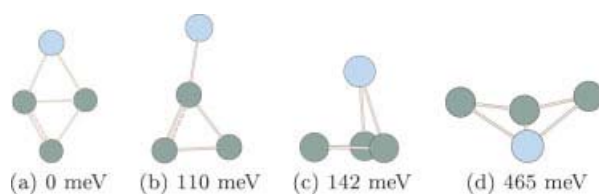


**FIGURE 2.** The lowest energy isomers of neutral  $\text{AgSi}_3$ . The numbers under the structures are the relative energies with respect to the lowest energy isomer of the same size. The Si and Ag atoms are shown in dark blue (dark gray) and light blue (light gray), respectively. [Color figure can be viewed in the online issue, which is available at [wileyonlinelibrary.com](http://wileyonlinelibrary.com).]

in the prescription above, but rejecting the outcome when the new Si atom is not placed in the half-plane opposite to the present position of the center of mass.

## 2.2. DFTB

The DFTB method is an approximate Kohn–Sham (KS) density functional theory (DFT) scheme [21–23]. It applies a linear combination of atomic orbitals representation of the KS orbitals, which can be derived within a variational treatment of an approximate KS energy functional. Although approximate, the method avoids any empirical parametrization by calculating the Hamiltonian and overlap matrices out of DFT-derived local atomic orbitals and corresponding atomic potentials. It includes ab initio concepts in relating the KS orbitals of the atomic configuration to a minimal basis of the localized atomic valence orbitals.

Using a minimal-basis representation of KS eigenstates and a superposition of optimized neutral-atom potentials and related charge densities for constructing the effective many-atom potential, all integrals are calculated within DFT. Self-consistency is included at the level of Mulliken charges rather than by self-consistently iterating electronic spin densities

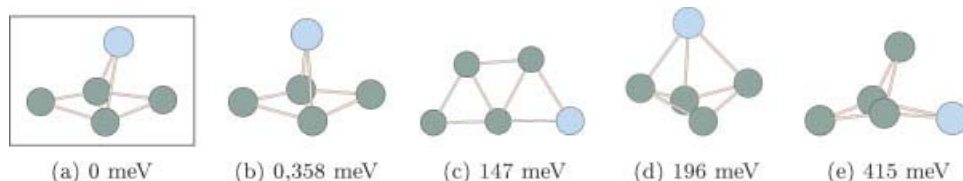


**FIGURE 3.** The lowest energy isomers of neutral  $\text{AgSi}_4$ . The numbers under the structures are the relative energies with respect to the lowest energy isomer of the same size. The Si and Ag atoms are shown in dark blue (dark gray) and light blue (light gray), respectively. [Color figure can be viewed in the online issue, which is available at [wileyonlinelibrary.com](http://wileyonlinelibrary.com).]

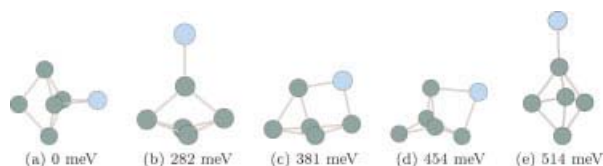


**FIGURE 4.** The lowest energy isomers of neutral AgSi<sub>5</sub>. The numbers under the structures are the relative energies with respect to the lowest energy isomer of the same size. The Si and Ag atoms are shown in dark blue (dark gray) and light blue (light gray), respectively. [Color figure can be viewed in the online issue, which is available at [wileyonlinelibrary.com](http://wileyonlinelibrary.com).]

and effective potentials. This leads to an approximate but still predictive scheme, with computational efficiency, reliability, and transferability.

### 2.3. COMPUTATIONAL DETAILS

To check the validity of our methodology, we first performed calculations on pure silicon clusters Si<sub>n</sub> ( $n = 2-20$ ) and hydrogenated silicon clusters Si<sub>n</sub>H<sub>m</sub> ( $n: 1-8; m: 1-3$ ) obtaining results in agreement with previous publications [24, 25]. It is worthwhile to stress that for each case studied by other authors, we reobtained all structures without any need to guide the search.

The procedure involved first carrying a random search with DFTB<sup>+</sup> [26] as function of aptitude. Then, the 10 best RSA structures in the sense of minimal energy were optimized locally with DFT computations based on the hybrid B3LYP functional, which consists of a combination of Becke's exchange functional B3 [27] with the nonlocal functional of Lee, Young, and Parr (LYP) [31], using the best available basis set for silver, 3-21G\* (6D,7F) implemented in the program GAUSSIAN03 [32]. The structures obtained were in general similar before and after the local

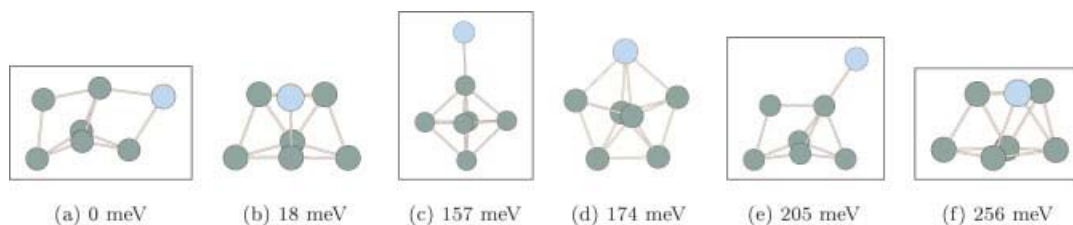


**FIGURE 5.** The lowest energy isomers of neutral AgSi<sub>6</sub>. The numbers under the structures are the relative energies with respect to the lowest energy isomer of the same size. The Si and Ag atoms are shown in dark blue (dark gray) and light blue (light gray), respectively. [Color figure can be viewed in the online issue, which is available at [wileyonlinelibrary.com](http://wileyonlinelibrary.com).]

optimization, only in a few cases did they change significantly. Furthermore, it never happened that a good DFTB<sup>+</sup> structure gave rise to a bad Gaussian structure, giving support to the use of DFTB as function of aptitude in the search.

## 3. Results and discussion

### 3.1. EQUILIBRIUM GEOMETRY

In this section, we present the results of our search for the lowest energy structures of AgSi<sub>n</sub> clusters, with  $n = 1-14$ . Figures 1–13 illustrate selected low-energy isomers for each case. All structures presented are stable. Harmonic vibrational frequencies were calculated in each case and if an imaginary vibrational mode (i.v.m.) was found, we carried out a relaxation along the coordinate of the i.v.m. to find a real local minimum.

The strategies attempted in the literature to find structures of AgSi<sub>n</sub> clusters proceeded up to now from previously known geometries. They either started from a (non-Ag) doped cluster replacing the dopant by a Ag atom [28], or from an homoatomic Si cluster [24] replacing one atom from the host cluster by Ag. In our case, thanks to the unbiasedness of the RSA algorithm, which does not rely on input geometries, in addition to all the structures previously reported in the literature we have found new geometries that we signal by an enclosing frame in Figs 1–12. For the AgSi<sub>14</sub> case, Fig. 13, we do not mark any of our structures because none have been reported yet.

The most stable isomer of each series is denoted (a) in each Figure. For these, we report in Table I the bond length from the Ag atom to the closest Si, the dipolar moment, and the binding energy with respect to those of the atomic species,  $E_{\text{Si}} = -287.8794 \text{ eV}$  and  $E_{\text{Ag}} = -5176.2788 \text{ eV}$ . It also

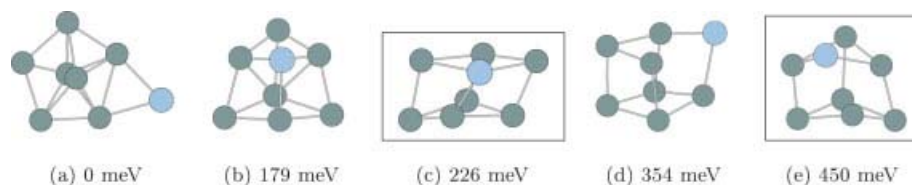


**FIGURE 6.** The lowest energy isomers of neutral  $\text{AgSi}_7$ . The numbers under the structures are the relative energies with respect to the lowest energy isomer of the same size. The Si and Ag atoms are shown in dark blue (dark gray) and light blue (light gray), respectively. [Color figure can be viewed in the online issue, which is available at [wileyonlinelibrary.com](http://wileyonlinelibrary.com).]

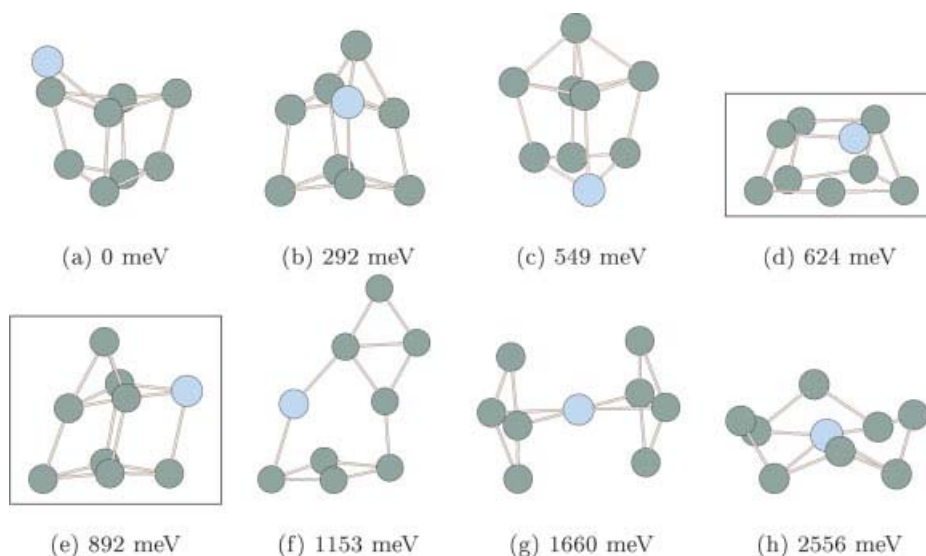


**FIGURE 7.** The lowest energy isomers of neutral  $\text{AgSi}_8$ . The numbers under the structures are the relative energies with respect to the lowest energy isomer of the same size. The Si and Ag atoms are shown in dark blue (dark gray) and light blue (light gray) respectively. [Color figure can be viewed in the online issue, which is available at [wileyonlinelibrary.com](http://wileyonlinelibrary.com).]

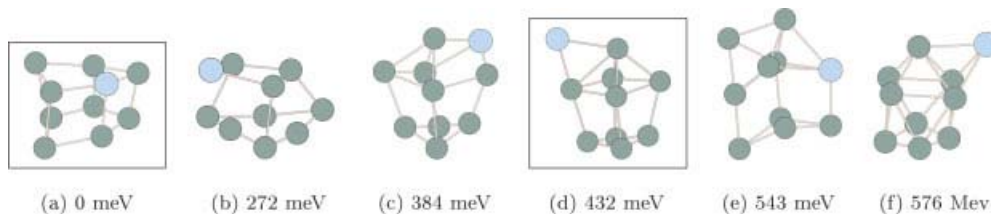


**FIGURE 8.** The lowest energy isomers of neutral  $\text{AgSi}_9$ . The numbers under the structures are the relative energies with respect to the lowest energy isomer of the same size. The Si and Ag atoms are shown in dark blue (dark gray) and light blue (light gray), respectively. [Color figure can be viewed in the online issue, which is available at [wileyonlinelibrary.com](http://wileyonlinelibrary.com).]

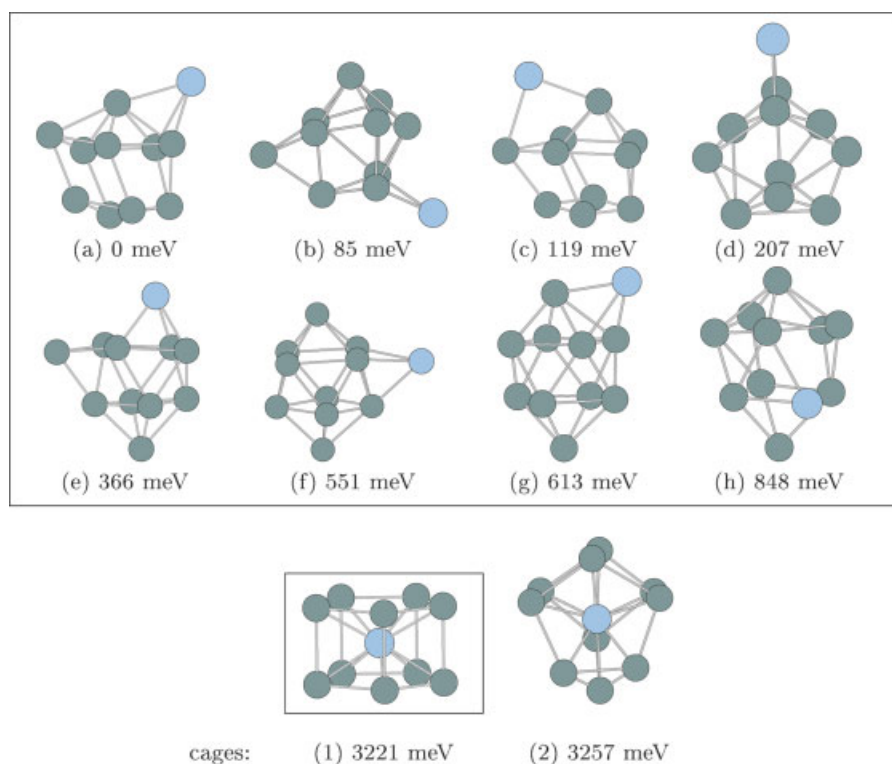


**FIGURE 9.** The lowest energy isomers of neutral  $\text{AgSi}_{10}$ . The numbers under the structures are the relative energies with respect to the lowest energy isomer of the same size. The Si and Ag atoms are shown in dark blue (dark gray) and light blue (light gray), respectively. [Color figure can be viewed in the online issue, which is available at [wileyonlinelibrary.com](http://wileyonlinelibrary.com).]

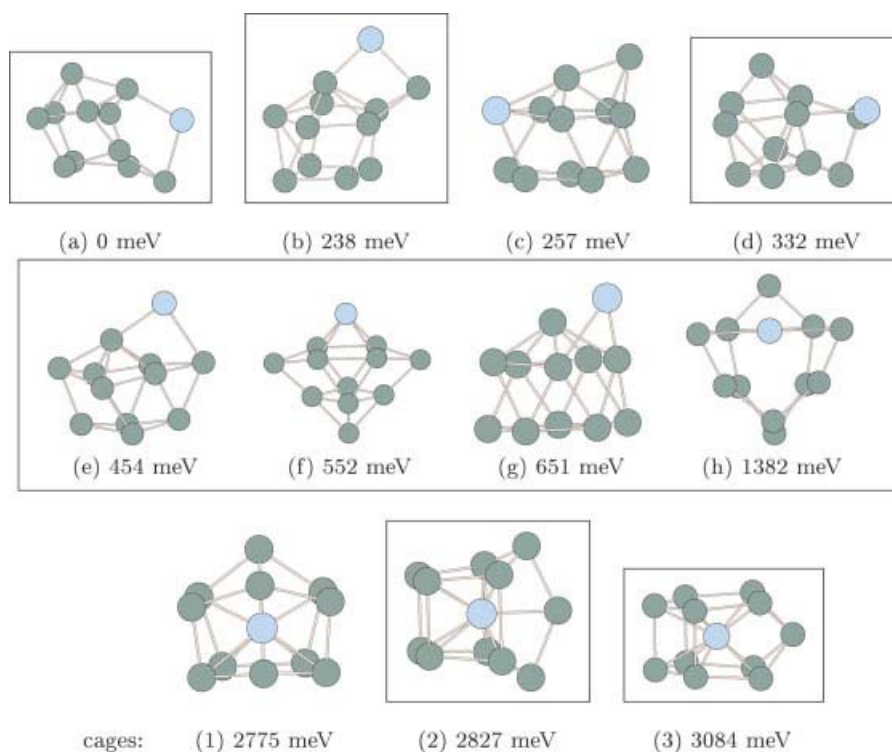


**FIGURE 10.** The lowest energy isomers of neutral  $\text{AgSi}_{11}$ . The numbers under the structures are the relative energies with respect to the lowest energy isomer of the same size. The Si and Ag atoms are shown in dark blue (dark gray) and light blue (light gray), respectively. [Color figure can be viewed in the online issue, which is available at [wileyonlinelibrary.com](http://wileyonlinelibrary.com).]

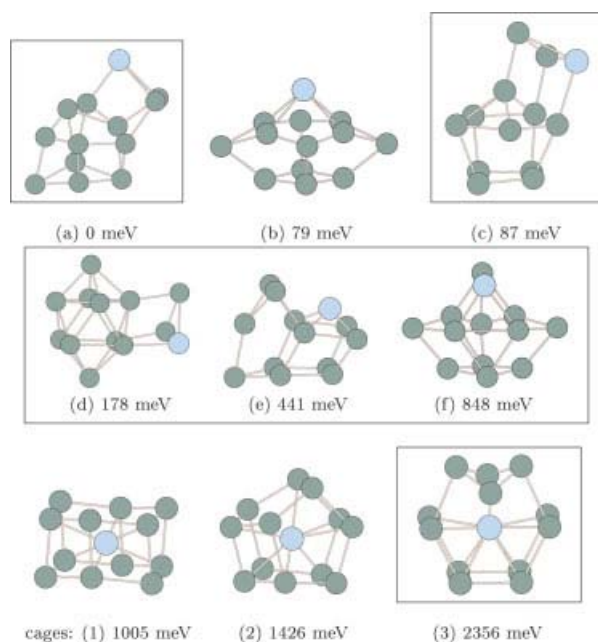


**FIGURE 11.** The lowest energy isomers of neutral  $\text{AgSi}_{12}$ . The numbers under the structures are the relative energies with respect to the lowest energy isomer of the same size. The Si and Ag atoms are shown in dark blue (dark gray) and light blue (light gray), respectively. [Color figure can be viewed in the online issue, which is available at [wileyonlinelibrary.com](http://wileyonlinelibrary.com).]

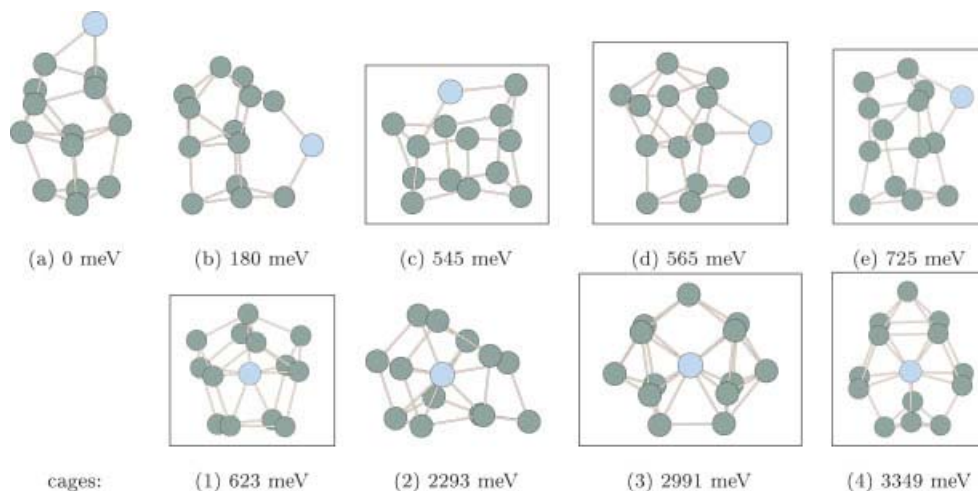


**FIGURE 12.** The lowest energy isomers of neutral  $\text{AgSi}_{13}$ . The numbers under the structures are the relative energies with respect to the lowest energy isomer of the same size. The Si and Ag atoms are shown in dark blue (dark gray) and light blue (light gray), respectively. [Color figure can be viewed in the online issue, which is available at [wileyonlinelibrary.com](http://wileyonlinelibrary.com).]

shows the energy to remove the Ag atom from the cluster,  $\Delta E_n = E_{\text{Ag}} + E_{\text{Si}_n} - E_{\text{AgSi}_n}$ , where  $E_{\text{AgSi}_n}$  is the energy of the cluster with  $n$  silicon atoms and  $E_{\text{Si}_n}$  the energy of the most stable pure  $\text{Si}_n$  cluster.

As mentioned before, for  $\text{AgSi}_{15}$ , Fig. 14, we only present the structures where the Ag atom is encapsulated. The most stable of these presents a BE of 70.66 eV,  $\alpha = 70 \text{ \AA}^3$ ,  $\mu = 1.2$  Debye, and an HOMO-LUMO gap of 1.2 eV. Table I does not include these numbers because in it we only report results for unconstrained minimum geometries.

We observe that the higher the cluster size  $n$ , the larger the fraction of cage structures with the metal atom in its interior, and the lower the relative energies of the corresponding endohedral structures. We also find that in agreement with previous reports [29], the first cage structures appear for  $n = 10$ , Fig. 9 (1). Although for  $\text{AgSi}_8$  the structures (g) and (h) seem to form a cage, the Ag atom actually serves as bond between two  $\text{Si}_4$  clusters.

Table I includes also the HOMO-LUMO gap (the energy difference between the highest occupied molecular orbital and the lowest unoccupied molecular orbital, regardless their spin polarization), which varies between 1.1 and 2.0 eV. Clusters with larger HOMO-LUMO gaps tend to be more stable and chemically inert. In our case this corresponds to the  $n = 5$ ,  $n = 7$ , and  $n = 10$  species. In Figure 15 we plot the HOMO-LUMO gap as function of the number of silicon atoms in the cluster, together with the hardness  $\eta$  [30], defined as the difference between

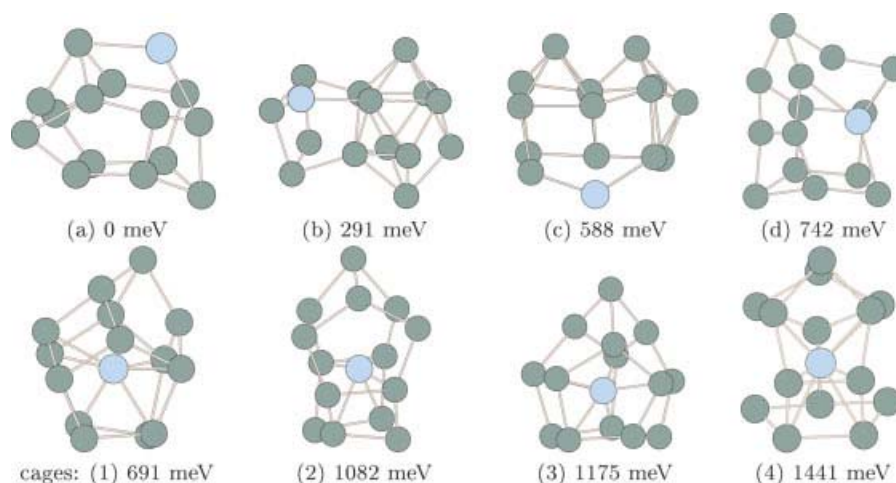


**FIGURE 13.** The lowest energy isomers of neutral AgSi<sub>14</sub>. The numbers under the structures are the relative energies with respect to the lowest energy isomer of the same size. The Si and Ag atoms are shown in dark blue (dark gray) and light blue (light gray), respectively. [Color figure can be viewed in the online issue, which is available at [wileyonlinelibrary.com](http://wileyonlinelibrary.com).]

the electron affinity and the ionization potential. It is apparent from this figure that both properties follow rather similar trends. This is a remarkable feature as two self-consistent calculations must be done for the hardness, one per ionic species, whereas only one for the HOMO-LUMO gap.

### 3.2. RELATIVE STABILITY

There are several concepts related to the relative stability of the AgSi<sub>n</sub> clusters. One of them is the binding energy between clusters differing by one Si atom. It follows from the equation AgSi<sub>n-1</sub> + AgSi<sub>n+1</sub> ↔ 2AgSi<sub>n</sub> that the condition for AgSi<sub>n</sub> stability with respect to its neighbors is that BE<sub>AgSi<sub>n-1</sub></sub> - 2BE<sub>AgSi<sub>n</sub></sub> + BE<sub>AgSi<sub>n+1</sub></sub> ≤ 0.

The binding energy of the AgSi<sub>n</sub> clusters grows essentially linearly with *n*, Figure 16(a), very well

described by a function BE(*n*) = 5*n* - 1.8. To enhance the deviations from this straight line, we plot on Figure 16(b) the ratio BE(*n*)/(5*n* - 1.8). We observe that indeed the linear relationship holds to better than 3%. The above condition for stability of AgSi<sub>n</sub> with respect to its neighbors is that the graphic of BE(*n*) must be convex at *n*.

However, there is here a more general question to address. Starting from a certain amount of available Si and Ag atoms at production time, we ask ourselves whether the system prefers to form (*y* - *x*) clusters of AgSi<sub>z</sub> rather than a mixture of (*y* - *z*) AgSi<sub>x</sub> + (*z* - *x*) AgSi<sub>y</sub> clusters, for any *x* < *z* < *y*. This aims at the relative stability of AgSi<sub>z</sub> with respect to arbitrarily smaller and larger clusters, for all *x* < *z* and *y* > *z*. It can easily be shown that the condition for the AgSi<sub>x</sub> + AgSi<sub>y</sub> mixture to be preferred over AgSi<sub>z</sub> is that the BE(*z*) be smaller than BE'(*z*),

**TABLE I**  
Properties of the lowest energy isomers of AgSi<sub>n</sub>: the bond distance from Ag to the closest Si atom, binding energy, Δ*E*<sub>n</sub> (see text), hardness, polarizability, HOMO-LUMO gap, and dipolar moment.

<i>n</i>	1	2	3	4	5	6	7	8	9	10	11	12	13	14
<i>d</i> (Å)	2.40	2.14	2.24	2.33	2.39	2.35	2.55	2.37	2.57	2.51	2.54	2.64	2.58	2.67
BE (eV)	3.00	8.19	12.83	17.89	23.17	28.01	32.64	37.40	42.36	47.46	51.83	56.55	61.80	66.47
Δ <i>E</i> (eV)	1.82	3.35	2.24	1.73	2.26	1.79	1.30	2.20	1.86	2.15	2.00	2.45	3.03	2.06
η (eV)	6.55	6.33	5.58	5.22	5.52	4.64	4.82	4.51	4.31	4.54	4.20	3.97	3.87	3.71
α (Å <sup>3</sup> )	83	140	133	151	181	221	241	271	294	317	352	391	411	432
hl gap(eV)	1.63	1.53	1.62	1.71	1.98	1.44	1.67	1.48	1.36	1.63	1.41	1.31	1.23	1.13
μ (D)	1.91	3.41	4.53	3.64	3.39	4.72	5.52	5.34	3.46	4.70	4.41	3.20	3.99	1.60

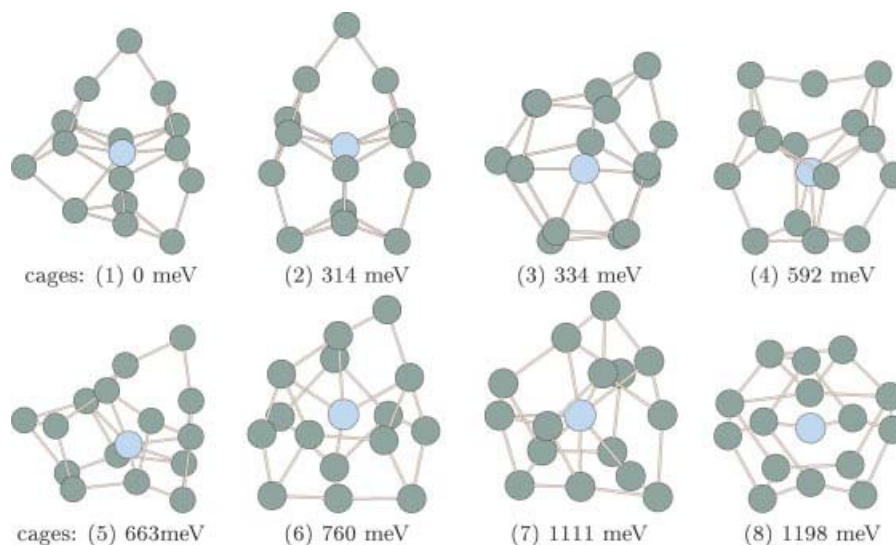


**FIGURE 14.** The lowest energy isomers of neutral  $\text{AgSi}_{15}$  “cages”. The numbers under the structures are the relative energies with respect to the lowest energy “cage” isomer. The Si and Ag atoms are shown in dark blue (dark gray) and light blue (light gray), respectively. [Color figure can be viewed in the online issue, which is available at [wileyonlinelibrary.com](http://wileyonlinelibrary.com).]

defined as the linear interpolation between  $\text{BE}(x)$  and  $\text{BE}(y)$ . Graphically, Figure 16(b), this means that clusters with BE below the convex envelope (CE), drawn with a dashed line, are energetically unfavored with respect to the clusters on the envelope. In particular, any cluster below a chord of the convex envelope will be energetically unpreferred with respect to those at the extrema of the chord. In this case, the stable species are predicted to be those with  $n = 2, 5, 10, 13$ .

This is further illustrated in Figure 17 where, as a measure of the relative energetic stability, we plot CE-BE: the difference between the linear interpolation, i.e. the value of the convex envelope CE, and the actual binding energy BE for each species. Although this plot indicates that  $\text{AgSi}_{10}$  is stable, as observed experimentally in [12], the energy differences are small. We conclude that energetic arguments themselves are not sufficient to explain the experimental abundance of the  $\text{AgSi}_7$  and  $\text{AgSi}_{10}$  configurations.

### 3.3. POLARIZABILITY

The static polarizability of isolated clusters is related to their optical properties and can be viewed as complementary information to their geometry and bonding nature. We calculated the static polarizabilities ( $\alpha_{xx}, \alpha_{yy}, \alpha_{zz}$ ) along the principal axes for all clusters. The average polarizabilities are extracted as  $\alpha = \sum_i \alpha_{ii}$ , and the directional polarizabilities  $\alpha_{ii}$  directly reflect the shape and size of the clusters.

The polarizability grows almost linearly with cluster size. This is best illustrated in the constancy of the polarizability per atom, Figure 18, supporting the approximate model of addition of atomic polarizabilities.

## 4. Metal Mono-Doped $\text{MSi}_{10}$ , $\text{MSi}_{11}$ , and $\text{MSi}_{12}$ Clusters

It is interesting to investigate the behavior of the lightest  $\text{AgSi}_n$  cage-like structures that we have found, when the dopant is another metal. We start

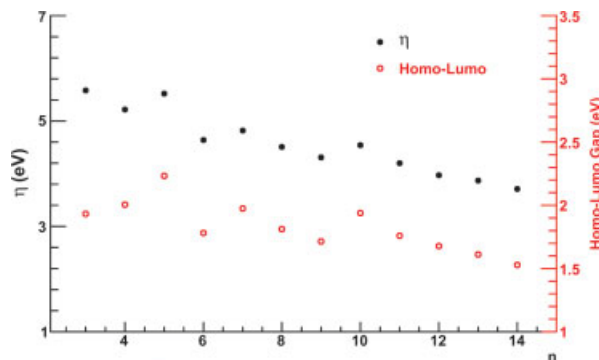


**FIGURE 15.** HOMO-LUMO gap (squares) and chemical hardness (triangles) for the lowest energy isomers of  $\text{AgSi}_n$ . [Color figure can be viewed in the online issue, which is available at [wileyonlinelibrary.com](http://wileyonlinelibrary.com).]

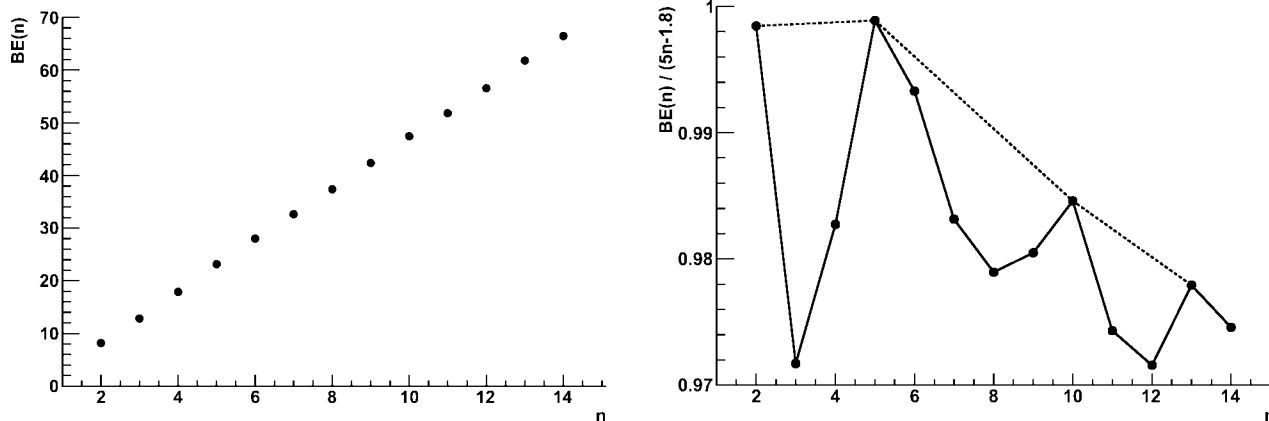


**FIGURE 16.** a. Left: Binding energy for the most stable  $\text{AgSi}_n$  isomer as a function of  $n$ . b. Right: Binding energy divided by  $\text{BE}(n) = 5n - 1.8$ , to enhance the deviations from a linear relation. We observe that these are less than 3%. The dashed line corresponds to the convex envelope (CE), discussed in the text.

from our most stable  $\text{AgSi}_{10}$ ,  $\text{AgSi}_{11}$ , and  $\text{AgSi}_{12}$  structures and replace the Ag atom by different X impurities,  $X = \text{Al, Si, Fe, Co, Ni, Cu,}$  and Au. The purpose of including Si itself as one of the options for X is to compare homonuclear to mono-doped  $n$ -atom clusters, with  $n = 11, 12, 13$ . For each of the 21 species we reoptimized the cluster geometry by minimizing its energy, and examined its stability via an analysis of the harmonic vibrational frequencies. Therefore, geometry and total energy for each stable cluster indeed correspond to a minimum.

As the 3-21G\* basis set is not available for all metals, we performed all electronic structure calculations in the B3LYP [27, 31] exchange-correlation

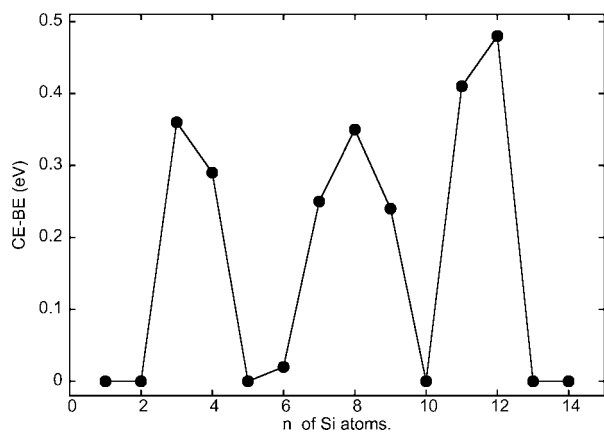


**FIGURE 17.** CE-BE: the difference between the convex envelope, dashed line in Figure 16(b), and the binding energy, solid line in Figure 16(b). The larger the value of CE-BE for a given  $n$ , the less energetically favored the production of the  $\text{AgSi}_n$  cluster.

functionals framework with the Stuttgart/Dresden effective core potentials [32]. We also verified that there are no significant differences with the  $\text{AgSi}_n$  results previously obtained with the 3-21G\* basis set.

The results are depicted in Figures 19–21, and summarized in Table II. We observe that, for  $X = \text{Si}$  or  $X = \text{Al}$ , we have lost the cage-like structure with an atom in the middle. Either the additional Si or Al atom prefers to be placed on the surface of the cluster rather than embedded inside. For all other dopants the favored geometry is still with the X-impurity inside of the cage, and we analyze the different cases below.

For the  $\text{XSi}_{10}$  clusters, most endohedral structures displayed in Figure 19 correspond to cage-like geometries with the  $X = \text{Co, Ni, Cu, Ag, Au}$

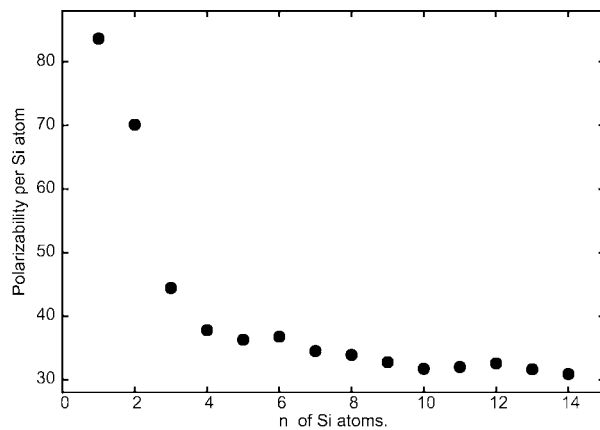


**FIGURE 18.** Polarizability per Si atom (in a.u.<sup>3</sup>) of the lowest energy isomers of  $\text{AgSi}_n$ .

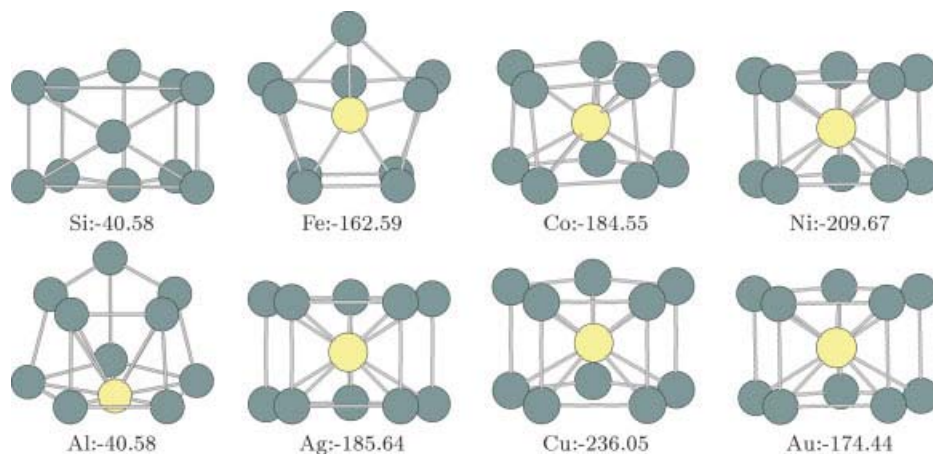


**FIGURE 19.**  $XSi_{10}$  cage-clusters ( $X = Al, Si, Fe, Co, Ni, Ag, Cu,$  and  $Au$ ) optimized with B3LYP/SDD. The numbers under the structures are the relative energies with respect to the lowest energy isomer of the same size. The Si and X atoms are shown in dark blue (dark gray) and yellow (light gray), respectively. [Color figure can be viewed in the online issue, which is available at [wileyonlinelibrary.com](http://wileyonlinelibrary.com).]

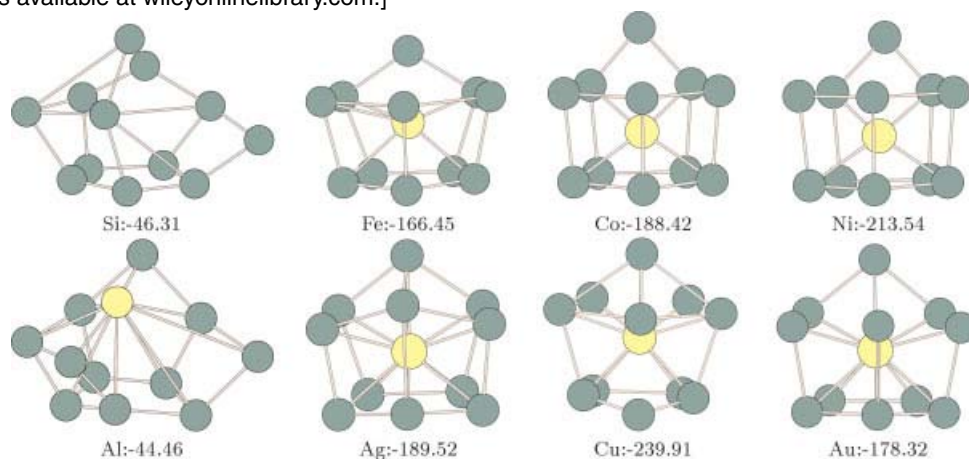


**FIGURE 20.**  $XSi_{11}$  cage-clusters ( $X = Al, Si, Fe, Co, Ni, Ag, Cu,$  and  $Au$ ) optimized with B3LYP/SDD. The numbers under the structures are the relative energies with respect to the lowest energy isomer of the same size. The Si and X atoms are shown in dark blue (dark gray) and yellow (light gray), respectively. [Color figure can be viewed in the online issue, which is available at [wileyonlinelibrary.com](http://wileyonlinelibrary.com).]

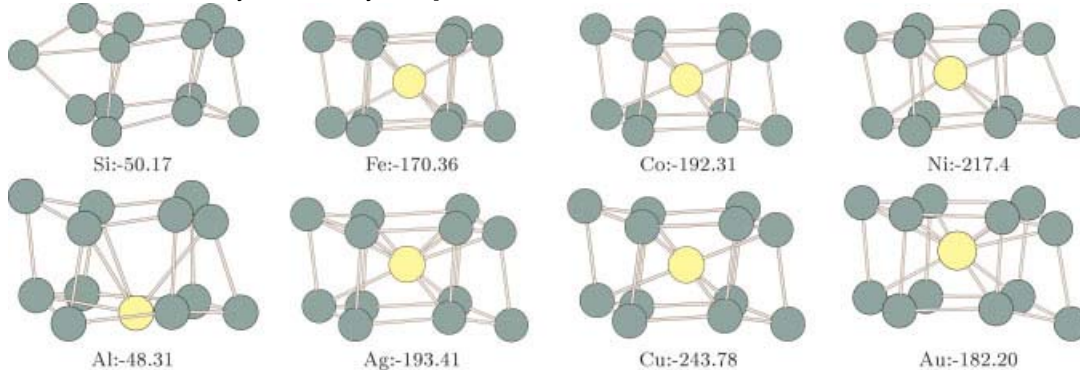


**FIGURE 21.**  $XSi_{12}$  cage-clusters ( $X = Al, Si, Fe, Co, Ni, Ag, Cu,$  and  $Au$ ) optimized with B3LYP/SDD. The numbers under the structures are the relative energies with respect to the lowest energy isomer of the same size. The Si and X atoms are shown in dark blue (dark gray) and yellow (light gray), respectively. [Color figure can be viewed in the online issue, which is available at [wileyonlinelibrary.com](http://wileyonlinelibrary.com).]

**TABLE II**  
Average binding distances, energy, polarizability, and dipolar moment of the most stable XSi<sub>n</sub> ( $n = 10-12$ ) cluster cages.

X	XSi <sub>10</sub>				XSi <sub>11</sub>				XSi <sub>12</sub>			
	$d$ (Å)	$E$ (a.u.)	$\alpha$ (a.u. <sup>3</sup> )	$\mu$ (D)	$d$ (Å)	$E$ (a.u.)	$\alpha$ (a.u. <sup>3</sup> )	$\mu$ (D)	$d$ (Å)	$E$ (a.u.)	$\alpha$ (a.u. <sup>3</sup> )	$\mu$ (D)
—		-38.49	362	1.21		-42.46	370	0.26		-46.31	407	0.0
Al	3.02	-40.58	378	1.12	3.39	-44.46	422	0.34	3.16	-48.31	436	1.20
Si	3.11	-42.40	388	1.54	3.42	-46.31	414	1.77	3.69	-50.17	444	2.32
Fe	2.46	-162.59	315	1.96	2.58	-166.45	349	0.69	2.75	-170.36	376	0.0
Co	2.44	-184.55	313	1.23	2.64	-188.42	373	0.37	2.72	-192.31	396	0.0
Ni	2.46	-209.67	324	1.21	2.41	-213.54	372	0.76	2.51	-217.40	395	1.13
Cu	2.50	-236.05	340	0.0	2.37	-239.91	366	0.31	2.54	-243.78	412	0.0
Ag	2.60	-185.64	359	0.95	2.72	-189.52	397	0.18	2.82	-193.41	428	0.35
Au	2.61	-174.44	356	1.03	2.70	-178.32	386	0.21	2.83	-182.20	426	1.17

impurities enclosed by two parallel slightly deformed pentagonal Si<sub>5</sub> rings. The exception is Fe, which forms an endohedral bicapped tetragonal, as already reported in [17]. The different properties of these XSi<sub>10</sub> clusters are shown in the first column of Table II. The average polarizabilities vary from 313 a.u.<sup>3</sup> (46 Å<sup>3</sup>) for CoSi<sub>10</sub> to 388 a.u.<sup>3</sup> (57 Å<sup>3</sup>) for SiSi<sub>10</sub>. The most symmetric structure is CuSi<sub>10</sub>, with  $\mu = 0.0$  Debye.

The XSi<sub>11</sub> cluster equilibrium geometries for X = Fe, Co, Ni, Cu, and Au, are similar to the

bipentagon sandwich-like X–Si<sub>10</sub> cluster above, with the additional Si atom capped on top of one of the pentagonal sides. It is remarkable that these structures are arrived at starting from AgSi<sub>11</sub>, which is in fact the only one that does not have a mono-capped pentagonal geometry (recall we are not considering AlSi<sub>n</sub>, which is altogether non cage-like). Our findings for CoSi<sub>11</sub> cluster are in agreement with those reported previously [33].

For the XSi<sub>12</sub> clusters, the cage-like geometry corresponds to the X impurity enclosed by two deformed hexagonal Si<sub>6</sub> rings. This hexagonal form, similar to that presented by the Si<sub>6</sub> cluster, is called “chair geometry” and is a structural element of the sp<sup>3</sup>-bonded diamond network of solid Si. We observe that Co, Fe, Cu, and Ag basically sit in the center of the original Si<sub>12</sub> bihexagonal cage. This is confirmed by the low dipole moment of these five species.

Table II summarizes for all the cases studied, the mean X–Si bond, the total energy, the polarizabilities, and the dipolar moment. We observe that the VIII-B elements bind more strongly than the I-B elements (AlSi<sub>n</sub> and SiSi<sub>n</sub> are kept out of this comparison because they are not encapsulated clusters).

In order to further understand the nature of the interactions of the impurity element with the cluster cage, we have plotted the HOMO–LUMO gap energy in eV regardless their spin polarization,<sup>1</sup> see Figure 22. The gap varies between 1.0 and 2.7 eV. They are all

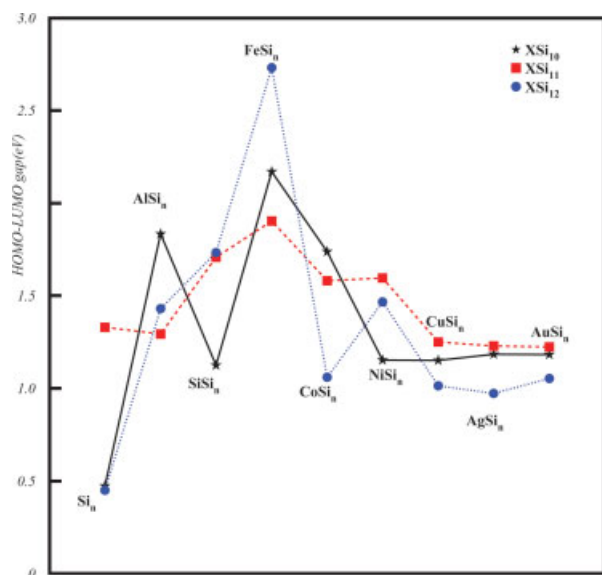


**FIGURE 22.** The HOMO–LUMO gap energy in eV for XSi<sub>n</sub> ( $n = 10, 11, 12$ ) clusters calculated using B3LYP/SDD. [Color figure can be viewed in the online issue, which is available at [wileyonlinelibrary.com](http://wileyonlinelibrary.com).]

<sup>1</sup>Extensive tests to check the implication of spin effects have been performed by Gueorguiev et al. [17, 18]. It was concluded that they do not play a significant role in the characterization of properties when the cluster contains only one transition metal atom.

larger than the nondoped  $\text{Si}_n$  case, allowing to conclude that the addition of the metal atom stabilizes the clusters.

## 5. Concluding Remarks

In this note, we have carried out a systematic search of equilibrium structures of  $\text{AgSi}_n$  ( $n = 1, 15$ ) clusters, applying the Random Search Algorithm (RSA) with the DFTB formalism for the energy calculation.

Our results strongly suggest that the approximate DFTB approach is accurate enough, while hundreds of times faster than *ab initio* methods, to provide an excellent first step in a predictor/corrector scheme for systematic cluster structure mapping. The attained RSA geometries were then optimized locally with B3LYP/3-21G\*. All the structures found are stable ones. Thanks to the unbiased nature of the RSA approach, we have found new structures in addition to all those previously reported in the literature.

From a study of the relative stability along the series, we conclude that there is no solid energetic argument to explain the experimental abundance of  $\text{AgSi}_7$  and  $\text{AgSi}_{10}$  observed by Jager and co-workers [12], although for  $\text{AgSi}_{10}$  we find it to be marginally more stable than its neighbors. In this sense we agree with Gueorguiev [17] in that there are stable endohedral structures for  $\text{AgSi}_{10}$ , and disagree with Zhang et al. [19], who report that  $\text{AgSi}_7$  has relatively stable isomers. We observe that the  $\text{AgSi}_n$  series satisfies the approximate model of addition of atomic polarizabilities and that the HOMO-LUMO gap and the hardness follow similar trends.

Geometries with encapsulated metal have been proposed in the past for many metal-silicon clusters. We have studied structures with up to 15 Si atoms, and found that it is not possible to fully enclose the metal dopant with cluster sizes smaller than 10. For larger sizes, stable encapsulated clusters appear but they are not the lowest lying isomers.

We also studied the properties of cage-like geometries when the Ag atom is replaced by other metals. We found, in agreement with the bibliography, that the average polarizabilities span values between 47–57 Å<sup>3</sup> for  $\text{XSi}_{10}$ , 52–59 Å<sup>3</sup> for  $\text{XSi}_{11}$  and 56–64 Å<sup>3</sup> for  $\text{XSi}_{12}$ . For a given cluster size, replacing the dopant metal changes the polarizability up to 15%, the heavier the metal, the larger the polarizability. This is consistent with heavier atoms being larger, the

increased volume of the  $\text{XSi}_n$  cluster corresponding to an augmented average polarizability.

The study of Si clusters stabilized by metal-encapsulation is in its infancy, but they have enormous potential for the assembly of new materials that are intermediate phases between pure silicon and metal silicides. We expect that the selection of the endohedral metal atom could act as a tunable building block permitting to control technologically relevant physical properties, such as the value of the HOMO-LUMO gap or the polarizability.

## ACKNOWLEDGMENTS

The authors gratefully acknowledge Bálint Aradi, G. Jungnickel, M. Elstner, and Th. Frauenheim, University of Paderborn, Germany, for the DFTB<sup>+</sup>-code and the silver-silicon Slater-Koster data.

## References

1. Morey, G. W. The properties of glass, 2nd ed., Reinhold: New York, 1954; Chapters 11 and 16.
2. Desurvire, E. *Phys Today* 1994, 47, 20.
3. Ho, K. M.; Shvartsburg, A. A.; Pan, B.; Lu, Z. Y.; Wang, C. Z.; Wacker, J. G.; Fye, J.; Jarrold, M. F. *Nature* 1998, 392, 582.
4. Honea, E. C.; Ogura, A.; Peale, D. R.; Felix, C.; Murray, C. A.; Raghavachari, K.; Sprenger, W. O.; Jarrold, M. F.; Brown, W. L. *J Chem Phys* 1999, 110, 12161.
5. Vasiliev, I.; Ogut, S.; Chelikowsky, J. R. *Phys Rev Lett* 1997, 78, 4805.
6. Singh, A. K.; Kumar, V.; Kawazoe, Y. *J Mater Chem* 2004, 14, 555; and references therein.
7. Hiura, H.; Miyazaki, T.; Kanayama, T. *Phys Rev Lett* 2001, 86, 1733.
8. Xiao, C.; Hagelberg, F.; Lester, W. A., Jr. *Phys Rev B* 2002, 66, 075425.
9. Kumar, V.; Kawazoe, Y. *Phys Rev Lett* 2001, 87, 045503.
10. Kumar, V.; Kawazoe, Y. *Phys Rev B* 2002, 65, 073404.
11. Liu, J.; Nagase, S. *Phys Rev Lett* 2003, 90, 115506.
12. Jaeger, J. B.; Jaeger, T. D.; Duncan, M. A. *J Phys Chem A* 2006, 110, 9310.
13. Scherer, J. J.; Paul, J. B.; Collier, C. P.; Saykally, R. J. *J Chem Phys* 1995, 102, 5190.
14. Scherer, J. J.; Paul, J. B.; Collier, C. P.; Saykally, R. J. *J Chem Phys* 1995, 103, 113.
15. Scherer, J. J.; Paul, J. B.; Collier, C. P.; Saykally, R. J. *J Chem Phys* 1995, 103, 9187.
16. Riekert, G.; Lamparter, P.; Steeb, S. Z. *Z Metallkunde* 1981, 72, 765.
17. Gueorguiev, G. K.; Pacheco, J. M.; Stafstrom, S.; Hultman, L. *Thin Solid Films* 2006, 515, 1192.
18. Gueorguiev, G. K.; Pacheco, J. M. *J Chem Phys* 2003, 119, 10313.
19. Zhang, P. F.; Han, J. G.; Pu, Q. R. *THEOCHEM* 2003, 634, 25.

20. Parr, R. G.; Yang, W. *Density-Functional Theory of Atoms and Molecules*; Oxford University Press: New York, 1989.
21. Seifert, G.; Eschrig, H.; Bieger, W. *Z Phys Chem (Leipzig)* 1986, 267, 529.
22. Seifert, G.; Porezag, D.; Frauenheim, T. *Int J Quantum Chem* 1996, 58, 185.
23. Elstner, M.; Porezag, D.; Jungnickel, G.; Elsner, J.; Haugk, M.; Frauenheim, T.; Suhai, S.; Seifert, G. *Phys Rev B* 1998, 58, 7260.
24. Oña, O.; Caputo, M. C.; Ferraro, M. B.; Facelli, J. C. *Phys. Rev A* 2005, 72, 53205.
25. Tiznado, W.; Oña, O.; Caputo, M. C.; Ferraro, M. B.; Fuentealba P. *J Chem Phys* 2005, 123, 214302.
26. <http://www.dftb.org>.
27. Becke, A. D. *J Chem Phys* 1993, 98, 1372.
28. Chuang, F.-C.; Hsieh, Y.-Y.; Hsu, C.-C.; Albao, M. A. *J Chem Phys* 2007, 127, 144313.
29. Guo, L.-J.; Zhao, G.-F.; Gu, Y.-Z.; Zeng, Z. *Phys Rev B* 2008, 77, 195417.
30. Parr, R. G.; Pearson, R. G. *J Am Chem Soc* 1983, 105, 7512.
31. Lee, C.; Yang, W.; Parr, R. G. *Phys Rev B* 1988, 27, 785.
32. Frisch, A. E.; Frisch, M. J.; Trucks, G. W. *GAUSSIAN 03 User's Reference*; Gaussian Inc.: Pittsburgh, PA, 2003.
33. Iwamatsu, M. *J Chem Phys* 2000, 112, 10976.